

Received February 22, 2022, accepted March 14, 2022, date of publication March 22, 2022, date of current version March 30, 2022.

Digital Object Identifier 10.1109/ACCESS.2022.3161490

Double Hybrid Tailsitter Unmanned Aerial Vehicle With Vertical Takeoff and Landing

ALYSSON NASCIMENTO DE LUCENA^{ID},
BRUNO MARQUES FERREIRA DA SILVA^{ID}, (Member, IEEE),
AND LUIZ MARCOS GARCIA GONÇALVES^{ID}, (Senior Member, IEEE)

Graduate program in Electrical and Computer Engineering Department, Universidade Federal do Rio Grande do Norte, Natal-RN 59076-200, Brazil

Corresponding author: Luiz Marcos Garcia Gonçalves (lmarcos@dca.ufrn.br)

The work of Alysson Nascimento De Lucena was supported in part by the Coordination of Superior Level Staff Improvement (CAPES), Brazil, under Grant 001. The work of Luiz Marcos Garcia Gonçalves was supported in part by the Pro-Alertas under Grant 311789/2021-8, and in part by the National Research Council (CNPq) under Grant 311640/2018-4.

ABSTRACT We propose a new double-hybrid concept and architectural design of a tailsitter unmanned aerial vehicle with vertical takeoff and landing capability. Basically, it consists of a modified flying wing with a single combustion powertrain set and a multirotor with 2 powertrain sets with electric motors. With the electric propellers fixed at the leading wing edge, the tailsitter has two standard surfaces for elevation control and two vertical stabilizers that are used to give the necessary direction on vertical takeoff and landing. We have designed, built, and tested a prototype based on this new double-hybrid concept, which spends less energy on vertical taking off and landing and also on horizontal flight, thus maximizing flight endurance and travelled distance. We performed several experimental tests starting with the aircraft on the ground in vertical positioning. These tests include executing vertical takeoffs and landing, transitions from vertical to horizontal flight modes and transitions back (from horizontal to vertical), and hovering, which were carried out successfully. Transitions fourth and back from combustion to multirotor are inherent to some of those flight mode transitions, which have also been performed smoothly. We also performed tests (in bench) to estimate the maximum flight duration, which has demonstrated about 32 minutes of endurance. To this end, the proposed and currently built double-hybrid prototype has proven to be functional as an effective hybrid UAV system.

INDEX TERMS Unmanned aerial vehicle, double hybrid tailsitter, architectural design, vertical takeoff and landing.

I. INTRODUCTION

The use of unmanned aerial vehicles (UAV) has becoming very popular as they can have applications in military or civilian fields. Several application tasks appear as images acquisition for surveillance and photogrammetry [24], [45], agriculture [10], plant detection and monitoring [16], smart cities [19], maritime surveillance [2], environmental monitoring [14], [35], disaster surveillance and monitoring [17], monitoring in livestock [5], and geological survey [30], among many others. According to their general physical characteristics they can be grouped simply in two widely known classes, with fixed or rotative wings. The ones with rotative wings can have single or multi-engines. Among the various types of multirotors, the most popular are quadcopters, as they

have good stability and control with less consumption of the energy matrix when compared to multirotors with more powertrains, such as hexacopters and octacopters. Multirotors with 3 arms are also used, however, a tilting mechanism is generally required in the tail power unit to cancel the free torque and carry out the yaw maneuver [22]. Carrying out a flight by means of a multirotor with only two powertrain sets is only possible with the help of control surfaces. This arrangement guarantees greater flight time endurance because less power is used. However, stability and control are affected as a consequence. Notice that each class has properties that make it less or more appealing for a specific type of application [37].

The need of combining characteristics of wing and rotative categories appears for some applications, which has inspired the development of another UAV type, called the hybrid ones. Indeed, a fixed-wing aircraft can reach great distances, but

The associate editor coordinating the review of this manuscript and approving it for publication was Engang Tian^{ID}.

cannot take off without having a runway. Nonetheless, this same aircraft cannot stop or fly at a very slow speed at any specific point. On the other hand, a rotary-wing aircraft does not have the same flight duration as a fixed-wing one. So, there are some task characteristic abilities that a multicopter or fixed-wing aircraft can carry separately, so it would be a good idea to combine them. Nonetheless, in addition to combining the types of aircraft, reconciling the advantages of more than one energy source increases the capabilities of the aircraft. For example, powertrains with electric motors have less vibration and more precise rotation control, while with external combustion engines. Despite the vibration and the response in the slower rotation control, they manage to deliver greater power due to the superiority of the energy density of liquid fuels in relation to batteries. Several models and prototypes have been developed in this class, some of them available as products nowadays [8], [11], [27], [28], [38], [47]. The most traditional and used models provide vertical takeoff and landing (VTOL) with multicopter and horizontal flight using a wing with a propeller system generally based on some fuel propulsion engine for longer endurance. In this case, the fuel tank in its weighting limit is able to provide more total energy than the electrical ones, despite having less maneuverability [3]. The multicopter is generally turned off during horizontal flight. For this, a simple approach is to use at least 3 electric rotors for VTOL and 1 or 2 combustion propellers for the horizontal flight [22].

A recent development is the tailsitter hybrid UAVs that can perform both VTOL and horizontal flight with only 2 powertrain sets [20], [23], [40], [42], in this case using electric engines. The use of only two electrical powertrains results in a longer time of flight in relation to the ones with three or more powertrains. Accordingly, flight endurance is enhanced by using a combustion engine and also by the better sustainability provided by the wings.

In this direction, the proposal of this work is to use cutting-edge technology and methods to develop a new concept of a double hybrid tailsitter type UAV that combines a multicopter (using 2 electric powertrain sets) for VTOL and a fixed (flying) wing with a single combustion powertrain set for long range missions. In this paper we deal with the architectural design, solving the problem of stability for taking off and landing and also we deal with the engines (and consequently flight modes) changing steps. To this end, we have developed a prototype that has been verified and proven to be effective, with a novel concept of structure that we named double hybrid. In these experiments, we performed several flights including takeoff, transition from vertical to horizontal flight mode, transition to hovering during horizontal flight, transition from horizontal to vertical flight, and back to ground (landing). All transitions and other flight modes (or steps) were tested. Particularly, transition tests from electric motors to the combustion engine for airplane mode flight (and the opposite) were successfully executed.

A first draft of the double hybrid tailsitter has been submitted as a patent [23], and some initial details on the design

and construction have been presented in our previous conference paper [25]. The work presented here is therefore a further enhancement of these previous versions in all aspects. We provide here new material, with more developments, experiments, and also with more details of the methodology described. To this end, we could not find similar approaches to ours in an extensive literature search considering its operation mode, as will be seen next in Section II.

Hence, the major contribution of our work is the new concept and architectural design of the double hybrid UAV prototype combining a double electrical powertrain set and combustion engine powertrain set with single propeller. Besides been tested in a controlled field, more extensive field tests for verifying flight endurance and the correctly working of autonomous flight model could not be performed due to pandemic time. Nonetheless, stability on taking off and landing close to the ground has been improved in relation to our previous work [25]. To date, technological aspects have been enhanced, with more powerful powertrain assemblies to expand the capacity of the embedded electronics and payload. So, besides the scientific and technical innovations we also have a product contribution, a working prototype consisting of a hybrid tailsitter wing with 1.20m of wingspan that can be applied for real-time transmission of images and video or other applications in the field.

This aircraft concept serves a wide range of applications where a multicopter UAV is not able to reach or a fixed wing UAV is unable to take-off due to lack of runway. Our solution is able to land and take off vertically, eliminating the need for a runway. It is also capable of reaching distances that a common multicopter would not be able to reach.

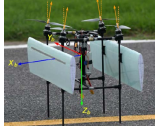




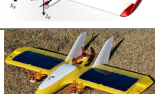
II. RELATED WORKS

From a first survey in the literature [34], we noticed an increase on the development of miniature UAVs, however, mainly treating separately the fixed-wing and VTOL UAV types. In the cited works it is observed several limitations relative to flexibility, payload, and time of flight for long range missions. Some of these limitations can be overcome by introducing a nonlinear mathematical model for the transitional flight as observed in a work dealing with a different aircraft model [40]. Physics laws are used to calculate the forces and moments acting on the UAV body and verified using simulations. Issues as aerodynamic effects of free airstream and propeller airstream are also treated and a CFD analysis is done. The trim point with respect to angle of attack, tilt angle, airspeed, thrust of tilt-rotor and coaxial fan is defined. Nevertheless, we could notice the application of this modeling in simulation, with definition of force and moment equations.

The literature also includes other survey papers on the design and flight control techniques for hybrid and convertible VTOL UAVs [12], [15], [18]. From these and from a further extensive search that we performed on the main bases (IEEE Xplore, Scopus, Web of Science, and Google Scholar), we selected the works that are most related to ours, which we summarize in Tables 1 and 2. Table 1 shows

some interesting models with 4 and 3 rotors, which are more widespread as they present greater stabilization efficiency during vertical flight, thus facilitating takeoff and landing [9], [21], [26], [30]. All of the models use electrical motors and have their mathematical modeling reported in the referred works (column reference). However, the works do not report the maximum allowed flight times for the aircraft for both vertical and horizontal flights.

TABLE 1. Hybrid VTOL with 3 and 4 propellers.

Picture	Reference	Configuration	Rotors
	[30]	Double wing	4
	[21]	Flying wing	4
	[9]	Double wing	4
	[26]	Flying wing	4
	[40]	Flying wing	3
	[7]	Flying wing	3

Regarding hybrid UAV with two or less powertrain sets, which are more straight related to ours, we found several works that are presented in Table 2. Several of them are wing type with the powertrains in front of the center of gravity. Some of them use a simple configuration, easier to manufacture with a rectangular wing [39], [44], and others use positive curling on the leading edge, in order to improve aerodynamics [6], [31], [36], [46]. We also found tailsitters with positive full-wing bending, which seek the best performance in horizontal flight aerodynamics [48]. Although models with flying wings predominate, models with a conventional configuration consisting of a fuselage and empennage are also studied [33], [41]. Also, models with only a single rotor are under study [13], [41], [43]. Due to the complexity of control, they use more complex structures, with fuselage and empennage, and vertical and horizontal stabilizers with control surfaces [43]. Or, when using flying wings, they need mechanisms such as small rotors to aid in stabilization and control [13].

The work of Oosedo *et al.* [28] shows one of the lowest energy consumption in flight prototypes, with a flying wing reaching 11.6 min of duration. In our experiments that will

TABLE 2. Hybrid VTOL with 2 (or less) propellers.

Picture	Ref	Config	Rotors	V/H-Time
	[44]	Wing	2	20 / No
	[39]	Wing	2	No / No
	[6], [36]	Wing	2	No / 29
	[31]	Wing	2	No / No
	[46]	Wing	2	No / No
	[48]	Wing	2	No / No
	[33]	Fuse/Empe	2	No / No
	[43]	Fuse/Empe	1	No / No
	[13]	Double Wing	1	No / 24.6
	[25]	Wing	2	5.2 / 27.5

be shown in Section V, we demonstrate that our work stands out in relation to tailsitters that uses only electric motors. By adding a combustion engine, we are able to increase the flight endurance, reaching in the worst case 23 min 41 sec with the used (default) fuel tank. Nonetheless, we are able to go up to 32 min with a larger fuel tank, which is possible to reach currently without losing lift as will be explained later in the experiments section. This advantage of our new concept, in relation to flight time endurance, also applies to the works of Kubo [20], Yanguo and Huanjin [47], Bapst *et al.* [4] and Wang *et al.* [41], [42].

Regarding the work of Bapst *et al.* [4] and the one of Ritz and D’Andrea [31], they comprise only a part of our work and do not report flight time endurance. Therefore, we could not perform a comparative analysis in this regard. However, as said, our experiments demonstrate that our work has greater flight time endurance compared to most tailsitter models with 2 electric powertrains. The Cyclone [6], [36] is the work that most resembles ours. In their first article [6], which discusses its construction, authors report that it has

only 0.88 m of wingspan, with a weight of 1.2 kg and do not detail which battery is used. They only talk about the voltage. Based on those, we figured out that it has to have a 4 cells battery, which is heavy. In their most recent article they report flights with 29 of duration, nonetheless, one can notice that the flight should be at a somewhat high speed in order to generate the necessary lift. In this same direction, just for the reader to have an idea, in a previous work [24] we developed a flying wing with 1.2 m of wingspan and weighting about 0.8 kg, which could fly for about 25 min.

III. HYBRID TAILSITTER CONCEPTUALIZATION

The main objective in the design of our hybrid tailsitter is to augment its flight endurance, which means the increase of flight time spending less energy, both in multirotor (vertical) and airplane mode. Hence, in order to provide a lower consumption of the electrical energy matrix (batteries), the electric powertrain sets are used only during takeoff and landing (vertical mode). They are aided by the mixed control surfaces (elevons) in order to guarantee vertical stability. In horizontal flight, we use a powertrain with a combustion engine that provides longer flight time when compared to our previous electrical one [23] and also to others from the literature, as seen in Section II. This will also be shown in Section V. Another important point in our current project is aerodynamics. According to the literature [1], the several types of drag that can occur on the surfaces of an aircraft moving through the air are, all of them, caused by two main sources (or phenomena): the shear stresses and the pressure distribution. Nevertheless, the total drag coefficient is directly related to the shape of the aircraft. In this regard, flying wings are considered aerodynamically more efficient, given that almost their entire structure is capable of generating lift. Furthermore, the absence of empennage and fuselage reduces the air resistance incident on the aircraft by reducing shear stresses and pressure distribution. It is noteworthy that, in an aircraft, the wing-fuselage combination has greater drag than the sum of the drag on the fuselage and the wing separately [1]. Given these facts, we chose the configuration in the form of a flying wing for our project, which results in greater flight endurance since it requires less traction to perform the flight. Equation 1 represents the total traction, where W is the weight of the aircraft, C_L is the lift coefficient, and C_D the total drag coefficient of the wing. The term $\frac{C_L}{C_D}$ is known as aerodynamic efficiency. Thus, using a flying wing instead of a traditional setup is another important point in our current project.

$$T_r = \frac{W}{(C_L/C_D)} \quad (1)$$

In view of the particularities of our project, the concept of hybrid tailsitter used here can be understood as a flying wing with mixed panels in positive deflection without dihedral, with two control surfaces that are mixed with a elevon configuration. When in airplane mode it is driven by a motor-propeller set with combustion engine and a propeller

in a common pusher configuration. In multirotor mode it has two powertrains in tractor configuration with electric motors and propellers positioned in the central part of each external panel. We installed a pair of vertical stabilizers with landing gear functionality at the junction of the panels. This tailsitter conceptualization can be seen in Figure 1.

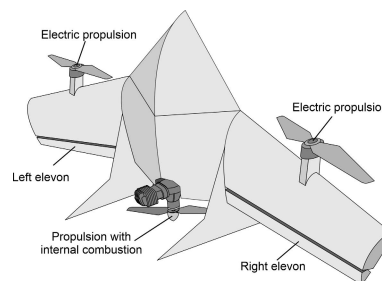


FIGURE 1. Illustration of basic embedded electronics for a remotely controlled standalone UAV.

Within this concept, we aim to develop a UAV able to perform a specific flight plan maximizing the flight time of each chosen mode. Each mission operation starts with the tailsitter at rest with the electric powertrains off and the combustion powertrain at idle as illustrated in Figure 2a. Then, takeoff starts in multirotor mode, with the electric motors activated and accelerated until reaching the lift necessary for the upward movement as seen in Figure 2b. The control and stabilization of the aircraft is aided by the elevons, when the aircraft reaches some desired altitude (5-6 meters), it starts the transition to airplane mode illustrated in Figure 2c. At this moment the electric motors are turned off and the flight continues with motion being generated by the thrust produced by the combustion engine simultaneously with the lift force generated by the wing. The aircraft remains in cruise flight until its mission has been accomplished and then it needs to land back. At this time a new transition to multirotor mode (vertical) is carried out. The combustion engine is put in idle state and the lift is solely produced by the electric engines again, as seen in Figure 2d. Then, the aircraft starts the vertical landing procedure, which is controlled through the electric motors and the mixed control surfaces as seen in Figure 2e. At this point, the hybrid tailsitter mission is completed with the landing procedure done, as indicated in Figure 2f.

Because of the versatility of this design, it is possible to perform a transition to multirotor mode (hovering) during some mission in airplane mode as seen in Figure 3a. The tailsitter can remain in hover flight or with very low displacement in order to better analyze some specific point, for example. Or, when in autonomous flight, to wait for some mission change during the mid-flight. Thus, after some detailed analysis of the location or new schedules, the tailsitter can make a new transition to airplane mode (Figure 3b) and follow the remaining of the mission accordingly.

In order for this concept of tailsitter with only two electric powertrain sets to be efficient, the control surfaces in the

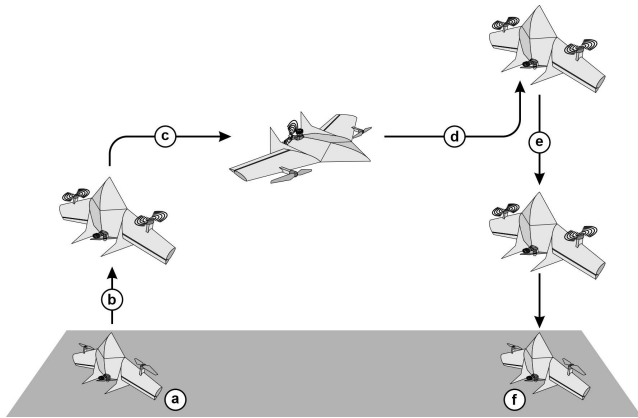


FIGURE 2. Illustration of basic functioning for vertical taking off and landing.

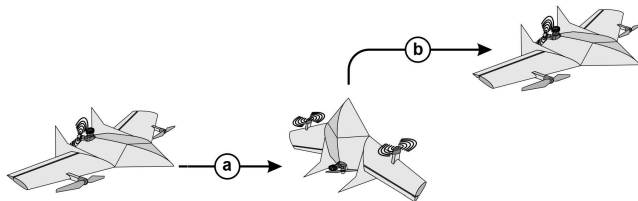


FIGURE 3. Illustration of a stop in mid-flight. This enables the aircraft to hover to, for example, capture some required scene detail or to wait for new mission assignments.

elevon configuration play a fundamental role in the stabilization and control of the aircraft. By varying the rotation of the engines, it is possible to perform the rolling, rotating, climbing and descending movements. The tilt and yaw movements are performed through the control surfaces in a mixed fashion. With the tailsitter maintaining support through the electric motors, a forward (Figure 4a) or retraction (Figure 4b) motion can be performed when the control surfaces are driven in the same direction. When this happens, the airflow that passes through the wing is deflected generating a counterforce to the deflected flow, producing a moment around the x axis.

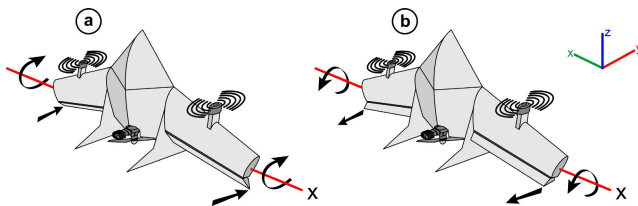


FIGURE 4. Forward (a) and retraction (b) movements.

The yaw movement in clockwise (Figure 5a) or counterclockwise (Figure 5b) are produced when the control surfaces are actuated in opposite directions. In this case, the airflow is deflected in different directions in each elevon, thus creating forces (with opposite directions) that produces a torque on the z axis.

To complete the allowed movements, the variation of the rotation of the electric motors, when equally accelerated or decelerated, provide the up and down movements.

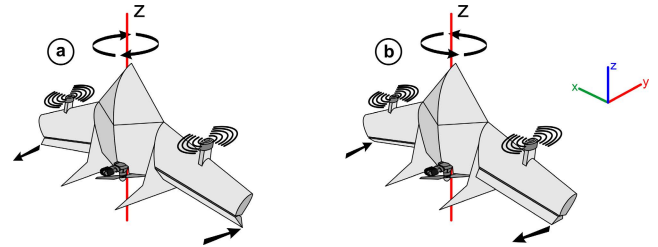


FIGURE 5. Clockwise (a) and counterclockwise (b) rotation movements.

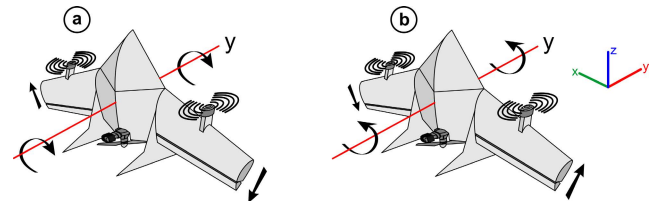


FIGURE 6. Scrolling movement to the right (a) and to the left (b).

When they vary their rotation with distinct accelerations, they promote the rolling movements around the y axis to the right (Figure 6a) or left (Figure 6b), depending on which rotation is the stronger.

IV. HYBRID TAILSITTER ARCHITECTURAL DESIGN

Our proposal is intended to be used in a versatile and easy way. The platform has been planned so that a single person is able to perform all autonomous flight scheduling operations, including piloting and real-time flight monitoring. The dimensions were chosen so that vehicular transport is possible using an economy car. Also, the chosen dimensions facilitate manual transport of all equipment, allowing thus access to hard to reach places without compromising the mission. Considering the operational requirements, the dimensions of the UAV have been devised as shown in Figure 7. Properties related to its dimensions are shown in Table 3. Its total weight (about 1.7 kg) is distributed according to Table 4 and can be better visualized through the pie chart shown in Figure 8.

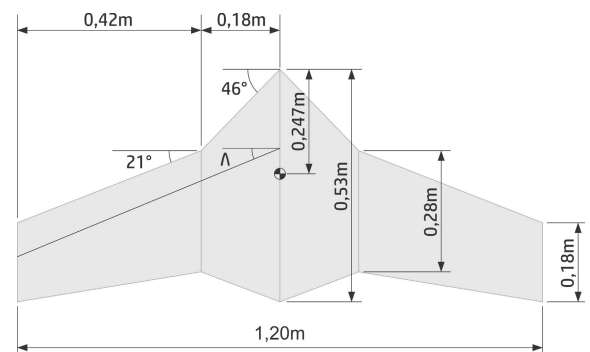


FIGURE 7. Basic measures of the of the VTOL-UAV (wing).

Despite the complexity involved in the tailsitter vertical and horizontal flight modes, the embedded system has a simple and reliable architecture, which has been designed to work with as few components as possible in order to promote

TABLE 3. Basic measures of the wing.

Wing area	0.339 m ²
Aspect ratio	4.28
Mean aerodynamic chord \bar{c}	0.26 m
Center of gravity	0.242 m
Wing sweep angle (Λ)	26.40°

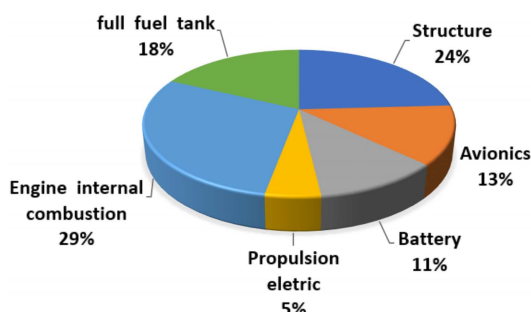


FIGURE 8. Hybrid tailsitter weight distribution by category.

stabilization and control. Although most experimental flights piloting were remotely performed by radio control in this work, an autopilot unit is present. It is the responsible component for automatically stabilizing and managing the order of change in flight modes between airplane and multirotor received through the remote pilot. The basic system architecture can be seen in Figure 9. We did not find in the literature such a similar architecture considering tailsitters with only one combustion engine assembly. However, if considering only the electric propulsion system with two control surfaces, similar approaches can be found [6], [36], [39], [44]. Nonetheless, it is one of the simplest when compared to tailsitter architectures with more than two powertrains [21], [26], or with more than two control surfaces [13]. Hence, the main difference between the architectural design on this work and the ones in the literature resides in the double hybrid concept, that is, it is hybrid in aircraft type (multirotor or vertical and airplane or horizontal) and in the types of powertrain used (electrical and combustion engines).

TABLE 4. Weight distribution of the hybrid tailsitter.

Structure	0.410 kg
Avionics	0.220 g
Battery	0.188 g
Propulsion electric	0.082 g
Combustion engine	0.495 g
Full fuel tank	0.305 g

A. EMBEDDED COMPONENTS ARCHITECTURE

The main embedded components of our tailsitter hybrid are seen in Table 5. An open source Pixhawk4 autopilot has been chosen to manage the flight system. It has a 32-bit FMU Cortex M7 main processor, 3-axis digital gyroscope, accelerometer, magnetometer, and barometer. The autopilot is aided by a GPS Ublox NEO-M8N with integrated compass

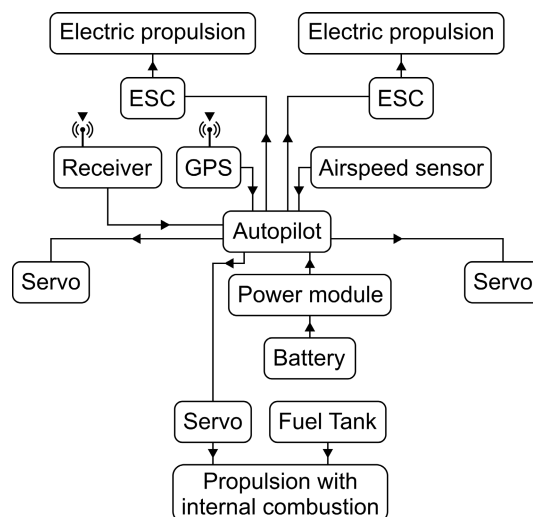


FIGURE 9. Illustration of the basic functioning of our hybrid tailsitter UAV - system architecture.

TABLE 5. Embedded system components.

Quantity	Item	Weight
1	Pixhawk 4	16 g
2	Brushless Motor Flashhobby 3530 1100 kv	74 g
2	Propeller slow flyer 1050	9 g
1	Receiver	14 g
1	GPS Ublox NEO-M8N With Compass	21 g
3	Servo Corona DS-239MG Digital Slim 4.6 kg	22 g
1	Airspeed sensor	25 g
2	ESC Brushless Speed Controller 50 A Skywalker	43 g
1	Distribution Board	5 g
1	Battery Turnigy Li-Po 2200 mAh 3S 11.1 V	188 g
1	Engine internal combustion Thunder Tiger 46 Pro	464.5 g
1	Propeller APC 10x7 Sport	31 g
1	Fuel Tank 295 ml	10 g

and a Holybro brand Pitot Tube digital speed sensor. The complete autopilot set is shown in Figure 10.

Due to the vertical take-off and landing characteristic, the powertrains with electric motors have as main function to offer static and dynamic thrust efficiency, despite being able to hover. Because the total mass of the aircraft is set at about 1.7 kg, the static thrust is estimated as 2.2 kg, which allows at least 0.5 kg of productive thrust when in multirotor mode. With this in mind we initially evaluate the technical characteristics of all parts available in the market in order to choose powertrains (electric motor and propeller), power supply (battery) and speed controllers (ESC). For that, we use the MotoCalc software for simulating the operation of each of the components, which gives as results their operation parameters (see Figure 11). These parameters are a starting point, and they will be later validated with bench tests and also in flight tests. During the simulations using MotoCalc,

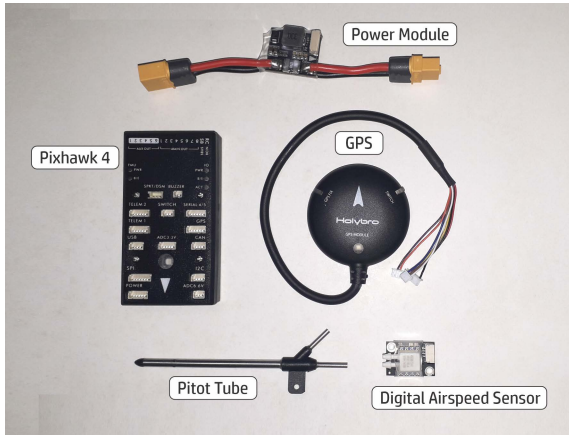


FIGURE 10. Autopilot set consisting on a power module, a pilot tube, a digital airspeed sensor and the Pixhawk. The latter component is responsible to run the autopilot software.

several combinations of components are tested, also taking into account the availability of purchase in the market, until reaching the choice that will be further presented in this work (Table 5). Subsequent tests, on the bench and finally in flight, will demonstrate the validity of the developed concept. The MotoCalc software is used for a previous assessment of the possible components, increasing the chances of success in the choice, thus avoiding the unnecessary expense in the acquisition of high-cost material. As the primary objective is to validate the concept, it is possible that new sets present better efficiency for the flight time, which does not invalidate the present work. New prototypes can be developed, with new components tested, in order to maximize the advantages of the new concept, including its mathematical modeling.

Hardware in the loop simulations demonstrated that a static thrust of 1.12 kg could provide 2.24 kg for the two electrical sets. From this initial evaluation, which will be further confirmed experimentally in our bench tests described in Section V, we could choose the electric motor that is a three-phase Flash-hobby model 3530 1100Kv brushless. Also, to complete the electrical propeller set, we have chosen the propeller Slow Flyer 1050 and an Electronic Speed Controller (ESC) model Skywalker with a maximum capacity of 50 amps. This system is powered by a LiPo battery of 3 cells (11.1v) with a capacity of 2200mAh. Here we also choose the combustion powertrain by way of a simulated analysis of its capacity in a straight level flight using the software AeroDesign Propeller Selector in order to verify its applicability. The experiments to confirm this choice will be shown further, in the Section V.

B. THE WING PROFILE

The airflow generated by the powertrain sets in multirotor mode crosses the wing structure in a similar way as in the horizontal flight mode. Using non-symmetrical aerodynamic profile could entail a force in the direction where the airflow exerts less pressure, as Figure 12 shows. A much more complex control model would have to be designed to compensate

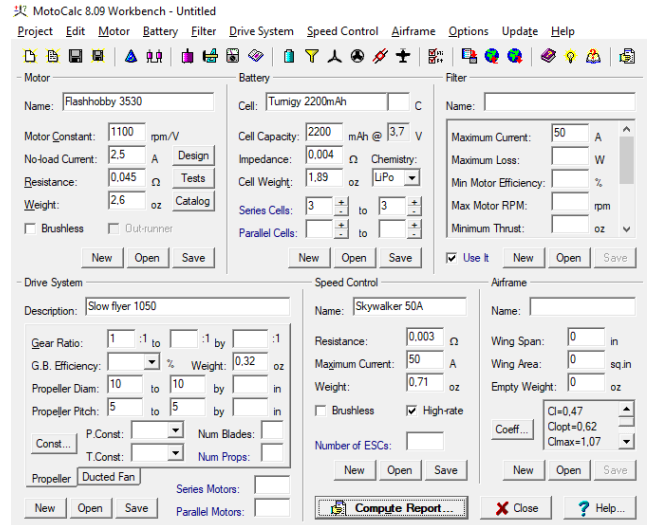


FIGURE 11. MotoCalc 8.09 workbench for powertrain sets evaluation.

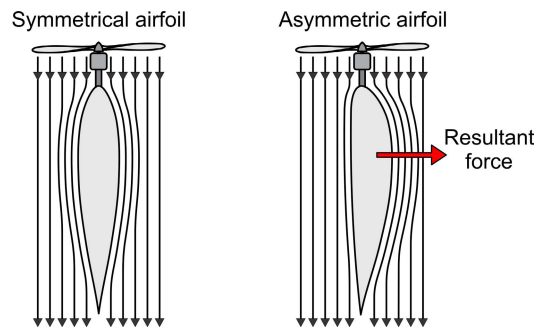


FIGURE 12. Symmetric and contrary forces acting on a UAV.

for the non-symmetrical profile in order to avoid instability during takeoff, landing, and vertical hovering. Hence, our design just requires the use of a symmetrical aerodynamic profile (left of Figure 12), to ensure that the hybrid tailsitter is not displaced to any direction during landing, take-off, and hover flight. This guarantees stability unless some wind gust occurs, in which case the autopilot stabilizes it. We notice that when using a non-symmetrical profile, the airflow that crosses the upper surface of the profile (right of Figure 12) has a greater velocity in relation to the lower surface flow. Therefore, according to the Bernoulli principle, the static pressure in the upper surface is lower than that of the lower surface, creating a force that would displace the aircraft during vertical flight. This is the principle that guarantees the flight of fixed-wing aircraft.

Thus, we previously selected three symmetrical profile models that avoid undesired displacement of the aircraft during vertical flight, in order to be further analyzed. These models are the NACA 012, EPPLER EA 6 (-1)-012, and S1012, which are shown in Figure 13. Further, in addition to the desired characteristic for vertical flight, it is also desirable that the chosen aerodynamic profile reconciles the highest lift coefficient value cl with the lowest drag coefficient value cd and moment coefficient cm during horizontal flight.

TABLE 6. Maximum values of forces and moments.

	l max	d max	d min	$m_{c/4}$ max
NACA 0012	36.59 N ($\alpha = 12^\circ$)	0.0189 N ($\alpha = 13^\circ$)	0.0031 N ($\alpha = 0^\circ$)	0.0347 N ($\alpha = 13^\circ$)
EPPLER EA 6 (-1) -012	36.23 N ($\alpha = 11^\circ$)	0.024 N ($\alpha = 12.5^\circ$)	0.0043 N ($\alpha = 0^\circ$)	0.0377 N ($\alpha = 12^\circ$)
S1012	35.50 N ($\alpha = 12^\circ$)	0.0180 N ($\alpha = 13^\circ$)	0.0056 N ($\alpha = 0^\circ$)	0.0539 N ($\alpha = 13^\circ$)

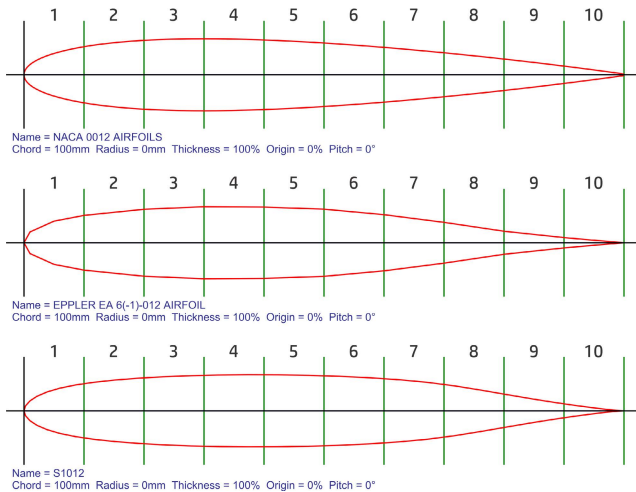


FIGURE 13. Symmetrical profiles NACA 0012, EPPLER EA 6 (-1) -012 and S1012.

Hence, we generate the characteristic curves for the lift coefficient, drag coefficient, moment coefficient, and for the aerodynamic efficiency using the Profili 2.30b software, for all three profiles. The characteristics curves are shown in Figures 14, 15, 16, and 17, respectively. They are determined as a function that varies according to the angle of attack (α), considering the value for the Reynolds number of 252,676 given by Equation 2.

$$Re = \frac{\rho \cdot v \cdot \bar{c}}{\mu} \tag{2}$$

where air density $\rho = 1.225 \text{ kg/m}^3$, the estimated velocity is $v = 15 \text{ m/s}$, and the dynamic viscosity coefficient $\mu = 1.8908 \times 10^{-5} \text{ kg/ms}$.

We evaluate performances for these aerodynamic forces and moments for choosing the right aerodynamic profile. Figure 18 illustrates these forces and moments that are generated on the given profiles for some given angles of attack (α). The lift force is represented by l , the drag force resulting from the shear forces acting on the entire surface of the profile is represented by d , and the component the resulting lift force is represented by R . In addition to these forces, a moment m is generated, which is usually calculated at the point that lies on the quarter of the chord from the leading edge. The lift and drag forces per wingspan unit generated by the profile and the moment around the aerodynamic center are expressed by Equations 3, 4 and 5 respectively, where v represents the undisturbed flow velocity and it is aligned with the relative

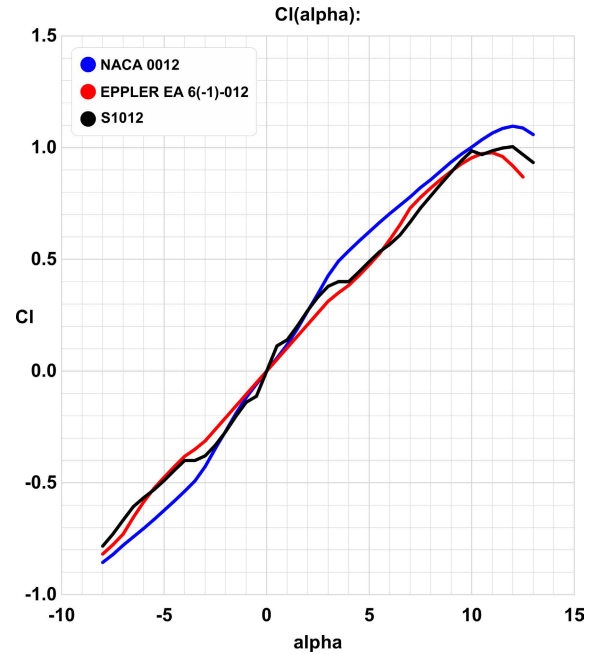


FIGURE 14. Characteristic curve of the lift coefficient.

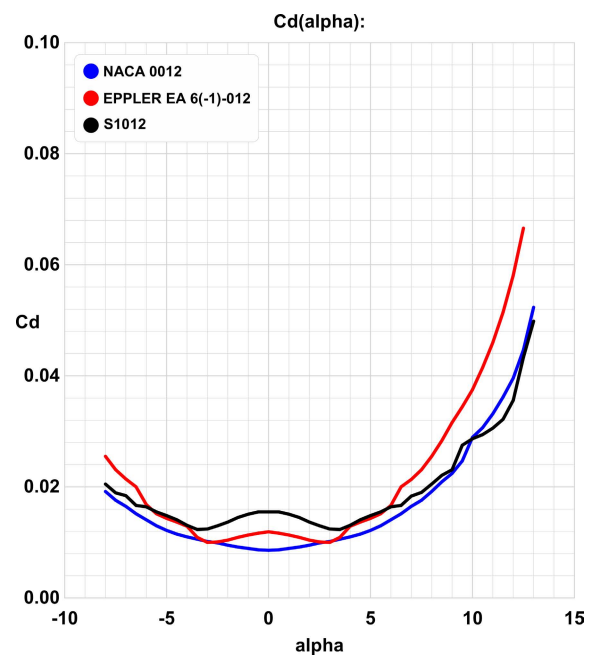


FIGURE 15. Characteristic curve of the drag coefficient.

wind direction, ρ is the air density, and c the profile string [1]. The coefficients C_l , C_d , and C_m have their values obtained from their respective plots [1]. The values referring to forces and moments are described in Table 6.

$$l = \frac{1}{2} + \rho \cdot v^2 \cdot c \cdot C_l \tag{3}$$

$$d = \frac{1}{2} + \rho \cdot v^2 \cdot c \cdot C_d \tag{4}$$

$$m_{c/4} = \frac{1}{2} + \rho \cdot v^2 \cdot c^2 \cdot C_m \tag{5}$$

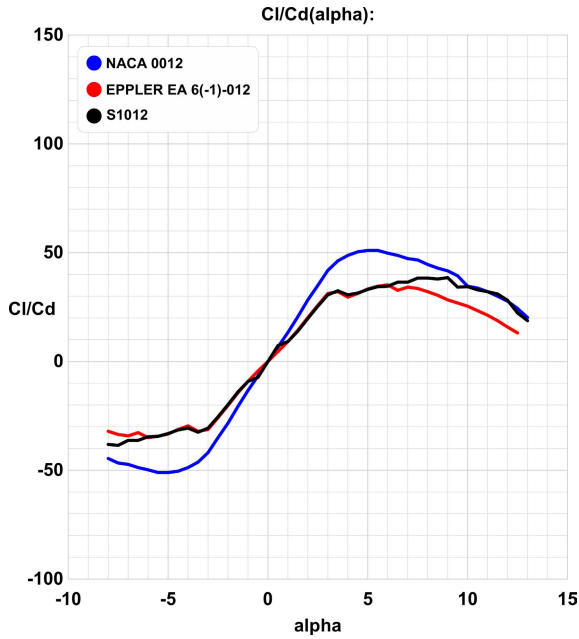


FIGURE 16. Characteristic curve of aerodynamic efficiency ($\frac{C_l}{C_d}$).

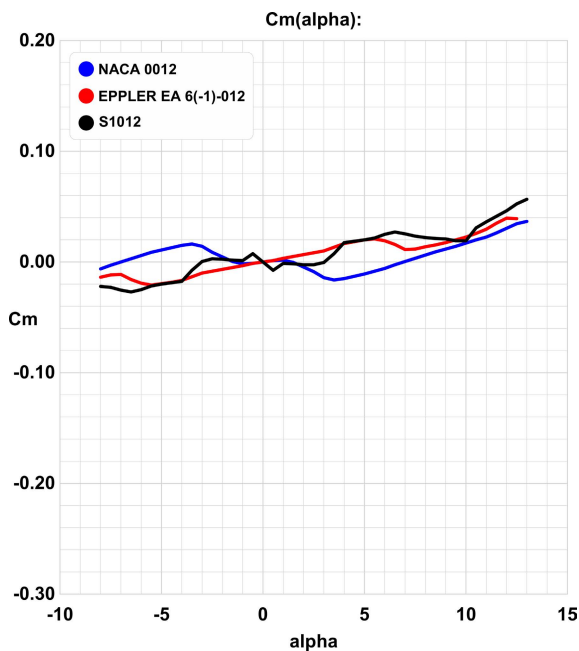


FIGURE 17. Characteristic curve for the moment coefficient.

During vertical takeoff, the tailsitter does not need to generate lift throughout the wing. However, during the transition to horizontal flight it is necessary for the wing to start producing lift as quickly as possible to ensure the effectiveness of the flight and, consequently, the controllability of the aircraft. Given this particularity, the characteristic curves graphs and the values shown in Table 6 are analyzed based on the given data. We choose the NACA 0012 profile mainly due to its greater capacity to generate the necessary initial lift on the transition to horizontal flight. We notice that the initial inclination α during takeoff starts at 90° in relation to the relative

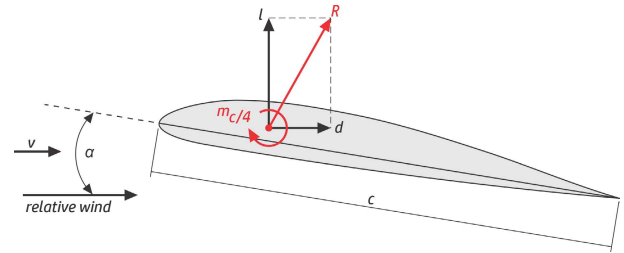


FIGURE 18. Aerodynamic forces and moments around the aerodynamic center.

TABLE 7. Stall data analysis for airfoil selection.

Profile	$C_{l(max)}$	Stall speed (m/s)
NACA 0012	0.8918	9.60
EPPLER EA 6(-1) - 012	0.8135	10.08
S1012	0.7975	10.18

wind (as shown in Figure 18) and decreases on transition. According to the plots of the lift coefficient characteristic curve, both Naca 0012 and S1012 profiles begin to generate lift when reaching 12° . However, the NACA 0012 has a higher lift coefficient, approximately 1.1 against 1.0 of the S1012. Conversely, when the aircraft starts the transition from horizontal to vertical flight, the NACA 0012 profile allows the lowest stall speed.

This speed is calculated through Equation 6, using the values expressed in Table 7. The lower the speed at the beginning of the transition to the vertical flight the lower the needed altitude to initiate landing or hovering operations. Other advantages presented by the NACA 0012 profile are the lower capacity to generate momentum, a maximum drag force closer to the most efficient profile (S1012), and a lower minimum drag force with $\alpha = 0^\circ$ (see Table 6). According to the plots in Figure 16, the NACA 0012 profile presents better values of aerodynamic efficiency coefficient, in addition to presenting less disturbed values. In addition to these measurable characteristics, the NACA 0012 profile is easier to fabricate, as can be noticed in Figure 13. In the referred figure, sections 8, 9 and 10 show a constant decrease in thickness. Besides, we notice that the NACA 0024 profile has a maximum thickness of 24% in relation to the chord. This value results in a slow flight when compared to the NACA 0012, since flying wing aircrafts need higher speeds than conventional aircraft with empennage. The flight speed guarantees the necessary amount of airflow under the control surfaces so that they act efficiently. Flying wings are unstable and loss of control can be catastrophic.

$$v_{stall} = \sqrt{\frac{2 \cdot W}{\rho \cdot S \cdot C_{l(max)}}} \quad (6)$$

In Equation 6, the value of $C_{l(max)}$ is approximated using Equation 7 and the term W is the aircraft weight, in Newtons. For a bowed wing in incompressible flight regime, the slope of the curve $C_l \times \alpha$ can be approximated through Equation 8, which also corrects the slope of the curve $cl \times \alpha$ for the profile

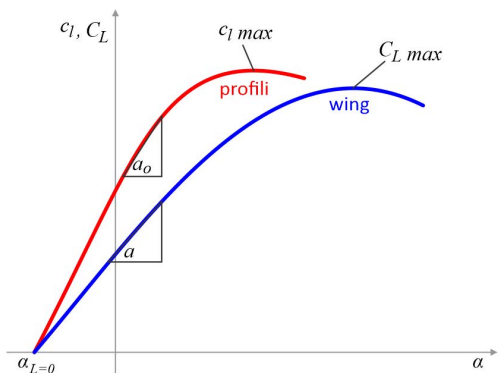


FIGURE 19. Comparison between the generic curves of a finite wing and an aerodynamic profile.

using the term $a_0 \cos \cdot \Delta$. When comparing the generic curves shown in Figure 19 we can see that the slope of the curve C_l x α for a finite wing will always be less than the slope of the profile [1].

$$C_l = a \cdot (\alpha - \alpha_{l=0}) \tag{7}$$

$$a = \frac{a_0 \cdot \cos \Delta}{\sqrt{1 + [(a_0 \cdot \cos \Delta) / (\pi \cdot AR)]^2} + (a_0 \cdot \cos \Delta) / (\pi \cdot AR)} \tag{8}$$

C. THE HYBRID TAILSITTER CONSTRUCTION

It is common to use more than one type of material for constructing the physical structure of a UAV in order to provide a light and resistant UAV. Our main structure uses polystyrene foam cut through a simple hot resistance cutting method. Basically, we fix two wing extremity molds with the chosen design of the aerodynamic profile on the sides of a massive polystyrene block. This mold is made of a 1mm thick alluminum. Then, a hot wire runs along the soffit and the extrados of the molds. Notice that the the central portions of each block will remain, which are the parts of each half wing panel as seen in Figure 20. We manufactured 4 independent panels and the vertical stabilizers and control surfaces using extruded polystyrene sheets with 4 mm thick.

Also, we use a round tube with diameter of $\frac{1}{2}$ inch for supporting the uprights of the electric motors. These uprights are made with a 3 mm thick marine polywood. Further, we reinforce the structure using fiberglass rods with 2 mm thick, which are added to the several parts as the leading edge, trailing edge, upper and lower part of the wing edges, and to the center of the vertical stabilizers. The manufacturing process is illustrated in Figure 21 and the final physical already mounted structure can be seen in Figure 22.

After the construction of the UAV main structure, we have installed the servos, ESCs, and cabling, internally. Then we have applied a self-adhesive vinyl coating on the wing and control surfaces. Finally, we put a series of equipments to finish the UAV, as autopilot system, radio control reception module, and the electric and combustion powertrain sets. The complete assembly of our hybrid tailsitter can be seen in Figure 23.

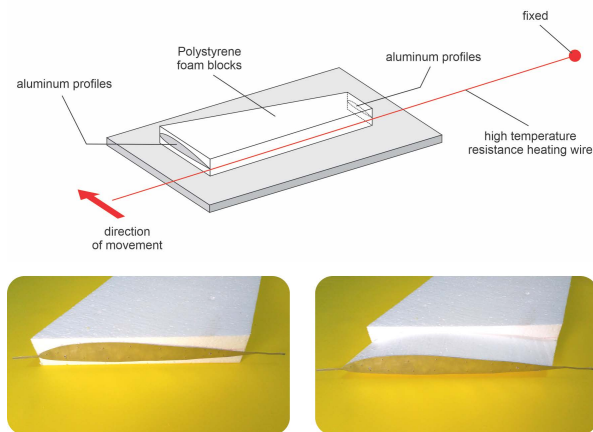


FIGURE 20. Wing making process through a simple hot resistance cutting method.

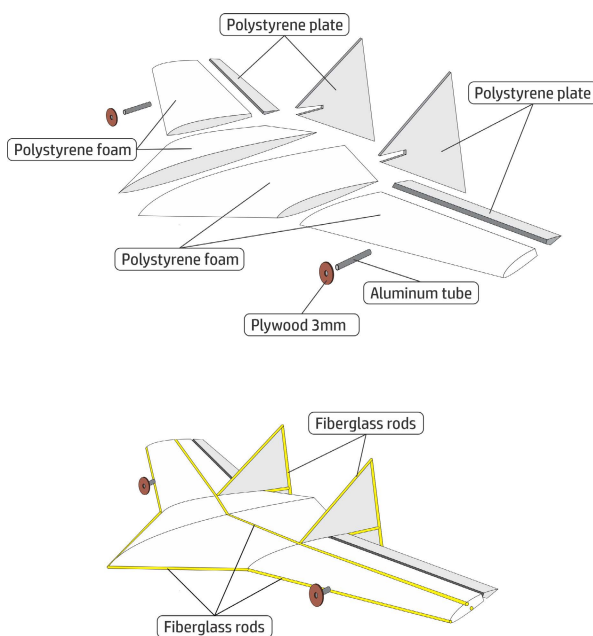


FIGURE 21. Basic materials and parts for manufacturing the main structure of the UAV.

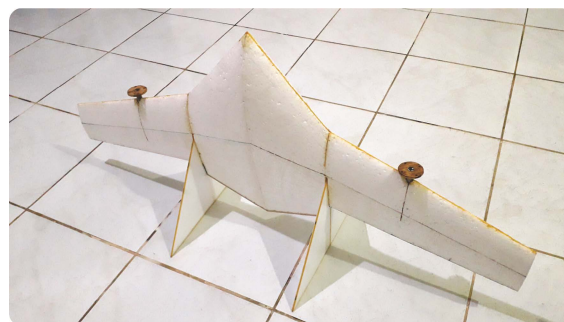


FIGURE 22. Materials and parts assembly of the main structure of the UAV.

V. EXPERIMENTS AND RESULTS

In our experimental setup, we have planed and executed several tests on the propellers, mechanics, electric



FIGURE 23. Complete assembly of the main UAV structure painted with a vinyl coating.

and electronics. In addition we have also performed a series of indoor and outdoor flight tests. In the initial tests, as seen in Figure 11, we evaluate the technical characteristics of the powertrain sets available in the market using the MotoCalc software, which allows us to choose the powertrain sets. Further, we assess the initial definition of the aircraft profile using simulation as well. Then, we have run hardware in the loop simulations, which demonstrates a static thrust of 1.12 kg that could provide 2.24 kg for the two electrical sets. Disregarding these initial setup that we have already described in Section IV, here we will put the remaining experiments and results (initial and/or final ones) that we believe completely validate our hybrid tailsitter.

A. BENCH TESTS FOR STRUCTURAL DESIGN AND CONSTRUCTION

We evaluate the powertrain sets individually on a bench to confirm the above simulated data with the aid of a digital precision scale. In addition, we calibrate the ESCs and proper balanced the propellers using a magnetic scale. From these tests, we determine values for the maximum static thrust as being 1.067 kg and 1.103 kg, which demonstrates that the MotoCalc simulation results were within the maximum expected variation of 10%. We select the smallest value between the two sets (1.067 kg) for calculating the maximum static thrust, which is obtained considering the estimated total mass of the aircraft. The resulting value is a 2.134 kg maximum static thrust, which results in an useful static thrust of 0.434 kg for the multirotor, also experimentally meeting our previously calculated value. Additionally, we have experimented to verify the combustion powertrain set in order to analyze its capacity during a straight and leveled flight. This test uses the required traction data that is given by Equation 1. We remember that the term C_l/C_d corresponds to the aerodynamic efficiency for a finite wing, with C_l being the lift coefficient and C_d the total drag coefficient. Thus, we basically calculate the characteristic curves for the available and required tractions. The used fuel is methanol from the Byron Premium Gen2 brand, which is combined with 10% nitromethane and 18 % synthetic oil. For this test, we calculate the maximum static thrust value as 2.380 kg. We use the simulation software *AeroDesign Propeller Selector* shown in Figure 25 to generate the available traction data. The required and available tractions according to velocity are

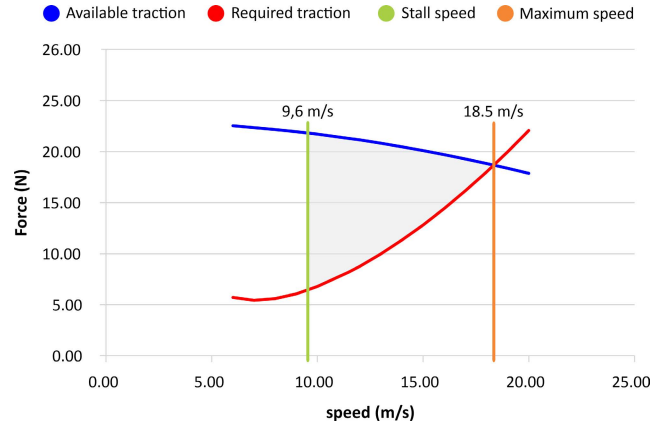


FIGURE 24. Curves for required and available traction data shown in Table 8.

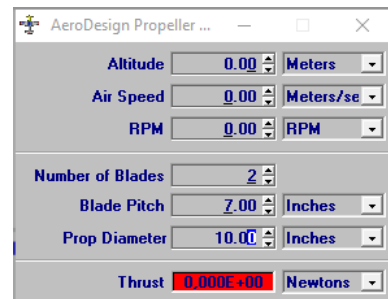


FIGURE 25. AeroDesign Propeller Selector.

TABLE 8. Data for available and required tractions.

V (m/s)	T_D (N)	T_R (N)
6	22.667	5.71
7	22.457	5.42
8	22.220	5.59
9	21.960	6.07
10	21.675	6.78
11	21.367	8.19
12	21.034	8.76
13	20.681	9.98
14	20.302	11.33
15	19.904	12.82
16	19.481	14.43
17	19.040	16.16
18	18.574	18.01
19	18.090	19.98
20	17.582	22.06

presented in Table 8, and its corresponding graph can be seen in Figure 24. Figure 24 also shows the maximum speed and the stall speed, which is calculated using Equation 6.

B. INDOOR FLIGHTS

To verify our UAV concept in practice, we manufactured a prototype initially without the combustion engine. Besides, in order to approximate it to the final desired behavior, we use powertrain sets with less thrust. For this, the prototype was built with two engines of the Sunnysky brand, model Anjo with 800kv, together with propellers of the GWS brand Slow Flyer model 10 × 4.5. Initial practical tests are carried out in

a closed place to avoid the interference of the wind, varying takeoffs and vertical landings as seen in Figure 26. They are mainly dedicated to the validation of the center of gravity, calibration of the ESCs, calibration of the Pixhawk 4 sensors, adjusting the control surfaces, and testing the radio control commands.

During takeoff, the hybrid tailsitter has demonstrated a larger acceleration in the right powertrain set, leaning the aircraft at beginning. Despite this inclination, the controller board performed a correction, and the problem was solved with a new calibration of the ESC through the Mission Planner software. As expected, the control surfaces need corrections, which we provided through the adjustments available in the radio control transmitter. During the flight, we performed forward and backward movements to test the center of gravity. We observed no problems and performed several more test flights until we achieved a perfect stabilization of the system. We also observe that the thrust generated by the electric power propellers is enough to keep the flight at hovering mode.

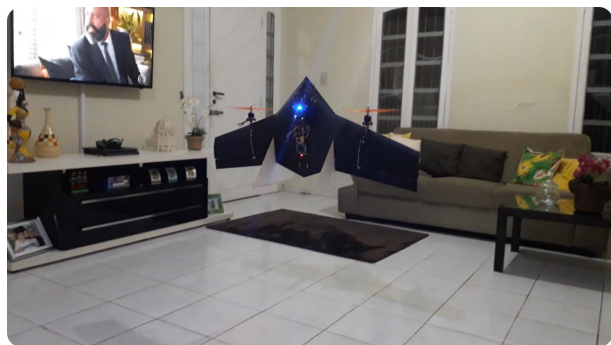


FIGURE 26. Indoor tests for stabilization without the combustion powertrain set.

Further, we notice some instabilities in the range from 0m to 0.60m of altitude. Nonetheless, the autopilot can provide the necessary corrections through the control surfaces, avoiding the crash of the aircraft. Above altitudes of 0.60m the aircraft proved to be stable, responding well to the movements of rolling, yawing and panting. The instability that occurs when the aircraft is below 0.60m is produced by the so called ground effect [29]. In order to correct this takeoff stability we just increase the takeoff speed. However, because the landing requires low descending speeds the same solution cannot be used. The option that we adopted for correcting landing instability was to increase the area of the control surfaces [29] of about 30%. After this correction, our prototype was ready to go to outdoor tests, as described next.

C. OUTDOOR FLIGHTS

Outdoor flights in a controlled field have been planned and executed including vertical takeoffs and landings, and transitions tests, starting with the same parameters as the indoor tests. The takeoffs have been executed in a stable manner, but the wind influence has made the landings even more unstable than in the indoor flights. Specifically, the descent is stable

until approximately 0.4m when it shows instability until touching the ground. Some displacement of the aircraft also happens during hover flight which is reduced by parallelizing the aircraft with the wind flow direction. Hence, takeoff and landing could be done without substantial problems, without damages to the prototype. Notice that in both cases (takeoff and landing) the aircraft uses only the electric powertrain sets, besides the combustion engine is on, however, its propeller is in neutral state.

After the tests with the electric power units, we performed tests with transition (from electric to fuelled and from vertical to horizontal, and vice-versa), in this case also using the combustion engine. The first test is the transition from vertical mode using electrical sets to horizontal flight mode with the fuelled set. When the aircraft starts from ground with full velocity and suddenly changes to fuelled, it does not loose altitude. However, if it is hovering and then it goes smoothly to airplane mode with combustion engine, it loses altitude. Such a test has been carried out as shown in Figure 27 starting with the tailsitter at approximately 5 m of altitude. The fuelled propeller is smoothly activated whereas the multirotor deactivated. During this transition, there was a loss of support generating a descent of approximately 4 m as it can be seen in the right picture of Figure 27.



FIGURE 27. Transition from hovering (multirotor) to airplane (fuelled) mode.

Further, a test on transition from horizontal (fuel) to vertical (electric) is shown in Figure 28, with the fuelled motor being smoothly deactivated while the multirotor mode is activated. The aircraft does a sudden climb due to the activation of the electric motors. The problem is that the aircraft should be as vertical as possible and with low velocity while the electric motors are activated and even if this is performed smoothly it suddenly loses its support. This means that it is necessary to reduce the speed of the aircraft as much as possible before the activation of the electric motors, and previously to the transition to hovering. During this transition, it is possible to observe that the aircraft has a tendency to tilt to the right. The possible cause is the torque effect generated by the combustion engine. However and fortunately, the autopilot performs the necessary corrections, aligning the aircraft. Hence, it returns to stabilization and performs the flight in hover mode, in this case using only the electric powertrain assemblies (the combustion engine keeps on, however in neutral status). The transition to multirotor mode has been stabilized at an altitude of approximately 6m. This is a little



FIGURE 28. Transition from airplane (fuelled) to hovering (multirotor) mode (left picture), just before landing (right picture).

far to ground, so some extra energy is consumed in order to execute landing, however, it is functional.

D. FLIGHT TIME ENDURANCE

The general rule is that fuelled motors have higher endurance and flight time than electrical motors mainly because in the limit size of the fuel reservoir, they can provide more total energy. The fuel tank size can be loaded up to this limit, as desired, albeit with less maneuverability [3]. Nonetheless, in order to determine the actual flight endurance, we have done a set of experiments to verify the time of operation of our UAV in order to compare the time-of-flight performance of each UAV mode. We carried out experimental tests in a bench test and in external flight. To assess the time-of-flight performance of the combustion engine-powered fixed-wing assembly, the consumption of the combustion powertrain is tested on the test bench shown in Figure 29. As a parameter for the analysis, we determined the cruise speed as the same as the takeoff speed, given by $V_t = 1.2 V_{stall}$ [32]. This value is considered conservative, because in the take-off performance, in addition to the forces for a straight and level flight, the friction force of the wheels with the ground is considered, which in our case is neglected. The calculated value was 11.52 m/s, rounded to 12.00 m/s, which results in a required traction of 8.76 N. These values present a safety margin in relation to the stall speed (9.6 m/s), and the powertrain can deliver up to 6.71 N, which provides a speed of 10.0 m/s. On the bench, 3 tests were performed, each one with the full fuel tank and the throttle adjustment, seeking to maintain the torque at 0.893 kg (8.7573 N). The average running time is 18 minutes and 27 seconds, which gives us an average consumption of 0.266 ml/s.

Next, we tested the flight time in flying wing mode on the same bench using the two electric powertrain sets. To calculate the cruise speed, we readjusted the stall speed, taking into account the reduction in weight due to the removal of the combustion power unit (0.495 kg), throttle actuation servo (0.022 kg) and fuel tank (0.01 kg), reaching the values of 7.958 m/s for the stall speed and 9.6 m/s for the cruise speed, which gives us a necessary thrust of 5.74 N (0.585 kg). LiPo batteries have a maximum safety limit for the voltage, 3.0 V for each cell, and during the tests the value of 3.2 V was established as a limit. To monitor the cells and determine the stopping time of the powertrain, a monitor with alarm was used. After three tests with the battery fully charged



FIGURE 29. Bench developed for testing flight time endurance.

TABLE 9. Flight endurance for the several configurations.

Type	Average time of flight
Multirotor with 2 propellers	5 min 14 sec
Electric tailsitter with 2 propellers	9 min 32 sec
Double hybrid tailsitter	18 min 27 sec

and used until the security alarm, the average flight time was established as being 9 minutes and 32 seconds.

To evaluate the performance of flight time in multirotor mode, external flights were performed. Each flight was performed with a fully charged battery and ended when one of the cells reached the 3.2 V limit, triggering the alarm. Since the evaluation aims to assess the performance of the aircraft, the powerplant, fuel tank and throttle actuation servo were removed from the prototype and the same compensation as above was made. After 3 flights in different wind conditions, we reached an average flight time of 5 minutes and 14 seconds.

A comparison between these times can be seen in Table 9, which demonstrates that the new UAV configuration presented in this work increases the flight time (endurance) while preserving the characteristics of a VTOL aircraft, with only 2 electric powertrain sets.

We emphasize that here the flight times are for each mode, separately, multi-rotor without combustion engine, tailsitter without combustion engine, and tailsitter with combustion engine. Actually, we can then add combustion engine time (18 min 27 sec) with the worst case of battery flight time (5 min 14 sec), which gives a total flight time of 23 min 41 sec. It is yet possible to increase the fuel tank, as we use

a default one. We have calculated that it supports more 0.15 kg, without losing maneuverability, which gives another 9 min of flight time. Thus, our aircraft can currently perform flights with up to 32 min 41 sec of duration. This is more than most of the times reported in the state of the art as seen above in Section II and is comparable to the work of Smeur et al. that most resembles ours [6], [36].

VI. DISCUSSIONS

We notice that with this size of aircraft the best and, in general, only available approach is to use empirical findings for the architectural design, including choosing the several components, handcrafting, and testing, until one prototype model works in some desired way. Hence, the size has been empirically defined for increasing endurance, based on the desired carrying weight of payload. The current wing size provides the minimum requirements for carrying our payload, using the chosen set of motors. Of course, the current size can be optimized, including a new set of motors, which is a matter of future work, not being the subject here. No software was used for the wing size definition. However, the profile was chosen based on simulation experiments. Still, the objective of the work is to create a new concept of Hybrid UAV that is able to maximize the flight time. For that, we have chosen the flying wing configuration and its dimensioning was performed with the help of an Excel spreadsheet, where we inserted input values for center chord, wing-end chord, span, bending angle for 1/4 of average chord, estimated weight, air density, and maximum lift coefficient for selected profile. The input values give us the stall speed, maximum lift coefficient for the wing and parasitic drag coefficient, which are used in order to meet the project requirements.

In addition to the aerodynamic parameters, the arrangement of the components influenced the choice of wing shape. The new concept developed can reach greater distances than a common multirotor, by way of using a double hybridization, which means doing hovering and also horizontal flights (first hybrid), and also by using two types of energy matrix, a LiPo battery, for the electric motors and liquid fuel, for the combustion engine. Liquid fuel has another advantage, when consumed during the flight, it reduces the total weight of the aircraft, increasing the flight time endurance. Because the combustion engine is at idle speed during multirotor mode flight, the torque generated by it is of low intensity, requiring small corrections of the control surfaces for its correction. This does not compromise the whole system's maneuverability, being corrected by the automatic pilot.

As explained above, with this size of aircraft, in general, the best and only available approach is to use empirical findings for the architectural design, including choosing the several components, handcrafting, and testing, until one prototype model works on some desired way. Hence, the size has been empirically defined for increasing endurance, based on the desired carrying weight of payload. The current wing size provides the minimum requirements for carrying our payload, using the chosen set of motors. Of course, the current size can

be optimized, including a new set of motors, which is a matter of future work, not being the subject here. No software was used for the wing size definition. However, the profile was chosen based on simulation experiments. Still, the objective of the work is to create a new concept of Hybrid UAV that is able to maximize the flight time, for that, we chose the flying wing configuration and its dimensioning was performed with the help of an Excel spreadsheet, where we inserted input values for: center chord, wing-end chord, span, bending angle for 1/4 of the average chord, estimated weight, air density, and maximum lift coefficient for selected profile. The input values give us the stall speed, maximum lift coefficient for the wing and parasitic drag coefficient, which are used in order to meet the project. In addition to the aerodynamic parameters, the arrangement of the components influenced the choice of wing shape.

Finally, it is widely known that there is not an exact mathematical model that can exactly represent this kind of (small) airplane, because even a small wind gust can make such a system unstable, and this is not feasible in simulators. Hence, modeling such behavior is difficult and it is preferable to go to a handcrafting for model creation and testing paradigm. This is the approach adopted in this work, with the models being handcrafted, based on our experience of more than 10 years of aircraft construction. Besides, as seen, after it proved to work we made further wind and software simulation tests to verify the several parts of our system and to enhance the initial model.

VII. CONCLUSION

We have proposed a new architectural model of a double hybrid tailsitter UAV including a prototype that proved to be functional, with an effective double hybrid system, in the sense that it has efficacy with most possible endurance. As discussed, it basically consists of a modified flying wing with a combustion powertrain set and a multirotor with 2 powertrain sets with electric motors. VTOL and hovering is done with electrical energy provided by batteries while the propeller for airplane mode uses a combustion engine. Our proposal uses two control surfaces for elevation control and two mixed vertical stabilizers to provide stability in vertical takeoff and landing. We performed several tests starting with the aircraft on the ground in vertical positioning. We have done several flights successfully including vertical takeoff and landing, transition to airplane flight (combustion), transition (back) to vertical flight (electrical) and hovering.

Therefore, our main contribution is the new concept and architectural design of the double hybrid tailsitter, which aims at augmenting the duration of missions while having VTOL and hovering capabilities. As technological contribution, with basis on our experiments and results, we have designed and built a working prototype that spends only the necessary electrical energy for vertical taking off and landing and also having more endurance on horizontal flight, in comparison with the state of the art, thus maximizing the total flight endurance. This new double hybrid concept can

be used in several applications including farther targets for multirotor UAV or ones in which a fixed wing UAV is unable to take-off due to lack of runway. Our solution is able to land and take off vertically, eliminating the need for a runway, it is also capable of reaching distances that a multirotor would not be able to reach, in addition to being able to perform hover flight during the mission.

Hence, our project has an unprecedented concept, which has never been tested before due to its mathematical modeling difficulty. The empirical experimentation approach used to design the aircraft proved to be effective, culminating in the construction and improvement of the prototype that from now on can be used in other studies that we will carry out in the future. Mathematical modeling is one such study. We did not find anything similar in the literature, in researches using the main publications databases (IEEE, Scopus, Web of Science, and Google Scholar). Furthermore, as a contribution to researchers in this field, we have provided here a full and detailed description of our architecture and prototype that we believe makes it easier for researchers to replicate our system, building their own prototype.

To date, we have built a last double hybrid tailsitter prototype with 1.50 m of wingspan equipped with a more powerful powertrain assemblies to expand the capacity of the embedded electronics for tests of real-time transmission of data and images. This last prototype has not been tested in the field, mainly due to the disruption caused by Covid-19 pandemic. Besides, as seen, our experiments have been carried out in indoor and outdoor scenarios. The current work focused on improving stability on landing close to the ground. Hence, more extensive field flights and experiments are yet necessary to more precisely determine the system endurance and also to perform autonomous flights with longer duration. Further tests on determining error between reference and performed trajectories will also be carried out using statistical measures based on embedded sensor data. Also, further research to autonomous flight execution including collision-avoidance and other issues will also be developed.

A. AUTHORS CONTRIBUTIONS

All authors have made substantial contributions to the conception or design of the work; the analysis, acquisition, and assembly of material and equipment; drafted the work and revised it critically for important intellectual content; and approved the version to be submitted, as described next. Alysso Nascimento De Lucena: Conceptualization, Methodology, Formal analysis and investigation, Writing-original draft preparation. Bruno Marques Ferreira Da Silva: Conceptualization, Methodology, Formal analysis and investigation, Writing-review and editing, Resources, Supervision. Luiz Marcos Garcia Gonçalves: Conceptualization, Methodology, Formal analysis and investigation, Writing-original draft preparation, Writing-review and editing, Funding acquisition, Resources, Supervision. In addition, all authors agree to be accountable for all aspects of the work in ensuring that questions related to the accuracy or integrity of any part of the

work are appropriately investigated and resolved. The authors declare that there are no conflicts of interests nor competing interests for this work. Data and design materials produced from or for this study can be requested to the authors by e-mail (see corresponding author e-mail).

REFERENCES

- [1] J. Anderson, *Fundamentals of Aerodynamics*, 5th ed. New York, NY, USA: McGraw-Hill, Feb. 2010.
- [2] F. A. A. Andrade, R. Storvold, and T. A. Johansen, "Autonomous UAV surveillance of a ship's path with MPC for maritime situational awareness," in *Proc. Int. Conf. Unmanned Aircr. Syst. (ICUAS)*, Jun. 2017, pp. 633–639.
- [3] J. Apeland, D. Pavlou, and T. Hemmingsen, "Suitability analysis of implementing a fuel cell on a multirotor drone," *J. Aerosp. Technol. Manage.*, vol. 12, p. e3220, Aug. 2020.
- [4] R. Bapst, R. Ritz, L. Meier, and M. Pollefeys, "Design and implementation of an unmanned tail-sitter," in *Proc. IEEE/RSJ Int. Conf. Intell. Robots Syst. (IROS)*, Sep. 2015, pp. 1885–1890.
- [5] M. Boon, A. Drijfhout, and S. Tesfamichael, "Comparison of a fixed-wing and multi-rotor UAV for environmental mapping applications: A case study," *ISPRS-Int. Arch. Photogramm., Remote Sens. Spatial Inf. Sci.*, vol. 42, pp. 47–54, Aug. 2017.
- [6] M. Bronz, E. J. Smeur, H. G. de Marina, and G. Hattenberger, *Development of a Fixed-Wing Mini UAV With Transitioning Flight Capability*. Reston, VA, USA: AIAA, 2017, vol. 35, ch. 3739, pp. 1–14. [Online]. Available: <https://arc.aiaa.org/doi/abs/10.2514/6.2017-3739>
- [7] S. J. Carlson and C. Papachristos, "The MiniHawk-VTOL: Design, modeling, and experiments of a rapidly-prototyped tiltrotor UAV," in *Proc. Int. Conf. Unmanned Aircr. Syst. (ICUAS)*, Jun. 2021, pp. 777–786.
- [8] E. Cetinsoy, S. Dikyar, C. Hancer, K. T. Oner, E. Sirimoglu, M. Unel, and M. F. Aksit, "Design and construction of a novel quad tilt-wing UAV," *Mechatronics*, vol. 22, no. 6, pp. 723–745, Sep. 2012.
- [9] V. S. Chipade, Abhishek, M. Kothari, and R. R. Chaudhari, "Systematic design methodology for development and flight testing of a variable pitch quadrotor biplane VTOL UAV for payload delivery," *Mechatronics*, vol. 55, pp. 94–114, Nov. 2018. [Online]. Available: <https://www.sciencedirect.com/science/article/pii/S0957415818301351>
- [10] L. Comba, A. Biglia, D. R. Aimonino, and P. Gay, "Unsupervised detection of vineyards by 3D point-cloud UAV photogrammetry for precision agriculture," *Comput. Electron. Agricult.*, vol. 155, pp. 84–95, Dec. 2018.
- [11] R. Czyba, M. Lemanowicz, Z. Gorol, and T. Kudala, "Construction prototyping, flight dynamics modeling, and aerodynamic analysis of hybrid VTOL unmanned aircraft," *J. Adv. Transp.*, vol. 2018, pp. 1–15, Oct. 2018.
- [12] S. Darvishpoor, J. Roshanian, A. Raissi, and M. Hassanalian, "Configurations, flight mechanisms, and applications of unmanned aerial systems: A review," *Prog. Aerosp. Sci.*, vol. 121, Feb. 2020, Art. no. 100694. [Online]. Available: <https://www.sciencedirect.com/science/article/pii/S0376042120301068>
- [13] C. De Wagter, R. Ruijsink, E. J. J. Smeur, K. G. van Hecke, F. van Tienen, E. van der Horst, and B. D. W. Remes, "Design, control, and visual navigation of the delftcopter vtol tail-sitter UAV," *J. Field Robot.*, vol. 35, no. 6, pp. 937–960, 2018. [Online]. Available: <https://onlinelibrary.wiley.com/doi/abs/10.1002/rob.21789>
- [14] B. Di Mauro, F. Fava, L. Ferrero, R. Garzonio, G. Baccolo, B. Delmonte, and R. Colombo, "Mineral dust impact on snow radiative properties in the European Alps combining ground, UAV, and satellite observations," *J. Geophys. Res., Atmos.*, vol. 120, no. 12, pp. 6080–6097, Jun. 2015.
- [15] G. J. J. Ducard and M. Allenspach, "Review of designs and flight control techniques of hybrid and convertible VTOL UAVs," *Aerosp. Sci. Technol.*, vol. 118, Nov. 2021, Art. no. 107035. [Online]. Available: <https://www.sciencedirect.com/science/article/pii/S1270963821005459>
- [16] P. Dvořák, J. Müllerová, T. Bartaloš, and J. Brůna, "Unmanned aerial vehicles for alien plant species detection and monitoring," *Int. Arch. Photogramm., Remote Sens. Spatial Inf. Sci.*, vol. 40, pp. 83–90, Aug. 2015.
- [17] K. Hasan, S. Newaz, and M. S. Ahsan, "Design and development of an aircraft type portable drone for surveillance and disaster management," *Int. J. Intell. Unmanned Syst.*, vol. 6, pp. 147–159, Jun. 2018.
- [18] M. Hassanalian and A. Abdelkefi, "Classifications, applications, and design challenges of drones: A review," *Progr. Aerosp. Sci.*, vol. 91, pp. 99–131, May 2017. [Online]. Available: <https://www.sciencedirect.com/science/article/pii/S0376042116301348>

- [19] H. Kim, L. Mokdad, and J. Ben-Othman, "Designing UAV surveillance frameworks for smart city and extensive ocean with differential perspectives," *IEEE Commun. Mag.*, vol. 56, no. 4, pp. 98–104, Apr. 2018.
- [20] D. Kubo, "Study on design and transitional flight of tail-sitting VTOL UAV," in *Proc. 25th Int. Congr. Aeronaut. Sci.*, 2006, pp. 1–12.
- [21] B. Li, W. Zhou, J. Sun, C.-Y. Wen, and C.-K. Chen, "Development of model predictive controller for a tail-sitter VTOL UAV in hover flight," *Sensors*, vol. 18, no. 9, p. 2859, Aug. 2018. [Online]. Available: <https://www.mdpi.com/1424-8220/18/9/2859>
- [22] A. N. Lucena, R. C. S. Freire-Júnior, and L. M. G. Gonçalves, "Unmanned aerial vehicle with hybrid lift and propulsion," in *Proc. Latin Amer. Robot. Symp. (LARS), Brazilian Symp. Robot. (SBR), Workshop Robot. Educ. (WRE)*, Oct. 2021, pp. 36–41.
- [23] A. N. Lucena, L. M. G. Gonçalves, J. C. P. Melo, R. C. S. F. Junior, J. F. D. de Rezende, D. L. F. Santos, D. S. da Pereira, L. P. W. de Oliveira, and P. J. Alsina, "Double hybrid unmanned aerial vehicle for vertical take-off and landing," *Invention Patent 10 2020 0 162 527*, Instituto Nacional da Propriedade Industrial-INPI, Rio de Janeiro, Brazil, (in Portuguese), 2020.
- [24] A. N. Lucena and L. M. G. Gonçalves, "Onboard instability correction of a flying wing unmanned aerial vehicle," in *Proc. Latin Amer. Robot. Symp. (LARS), Brazilian Symp. Robot. (SBR) Workshop Robot. Educ. (WRE)*, Nov. 2020, pp. 1–6.
- [25] A. N. Lucena and L. M. G. Gonçalves, "Towards a double hybrid VTOL UAV system," in *Proc. Latin Amer. Robot. Symp. (LARS), Brazilian Symp. Robot. (SBR) Workshop Robot. Educ. (WRE)*, Nov. 2020, pp. 1–6.
- [26] X. Lyu, H. Gu, Y. Wang, Z. Li, S. Shen, and F. Zhang, "Design and implementation of a quadrotor tail-sitter VTOL UAV," in *Proc. IEEE Int. Conf. Robot. Automat. (ICRA)*, May 2017, pp. 3924–3930.
- [27] J. M. O. Barth, J.-P. Condomines, M. Bronz, L. R. Lustosa, J.-M. Moschetta, C. Join, and M. Fliess, "Fixed-wing UAV with transitioning flight capabilities: Model-based or model-free control approach? A preliminary study," in *Proc. Int. Conf. Unmanned Aircr. Syst. (ICUAS)*, Dallas, TX, USA, Jun. 2018, pp. 1157–1164. [Online]. Available: <https://hal-enac.archives-ouvertes.fr/hal-01817515>
- [28] A. Oosedo, A. Konno, T. Matsumoto, K. Go, K. Masuko, and M. Uchiyama, "Design and attitude control of a quad-rotor tail-sitter vertical takeoff and landing unmanned aerial vehicle," *Adv. Robot.*, vol. 26, nos. 3–4, pp. 307–326, Jan. 2012.
- [29] D. P. Pulla, *A Study of Helicopter Aerodynamics in Ground Effect*, 1st ed. Columbus, OH, USA: The Ohio State Univ., 2006.
- [30] N. Raj, R. Banavar, Abhishek, and M. Kothari, "Attitude control of novel tail sitter: Swiveling biplane-quadrotor," *J. Guid., Control, Dyn.*, vol. 43, no. 3, pp. 599–607, Mar. 2020.
- [31] R. Ritz and R. D'Andrea, "A global controller for flying wing tail-sitter vehicles," in *Proc. IEEE Int. Conf. Robot. Automat. (ICRA)*, May 2017, pp. 2731–2738.
- [32] L. E. M. J. Rodrigues, *Fundamentals of Aeronautical Engineering*, 1st ed. Boston, MA, USA: Cengage Learning, (in Portuguese), Mar. 2013.
- [33] D. Rohr, M. Studiger, T. Stastny, N. N. R. J. Lawrance, and R. Siegwart, "Nonlinear model predictive velocity control of a VTOL tilting UAV," *IEEE Robot. Autom. Lett.*, vol. 6, no. 3, pp. 5776–5783, Jul. 2021.
- [34] A. S. Saeed, A. B. Younes, S. Islam, J. Dias, L. Seneviratne, and G. Cai, "A review on the platform design, dynamic modeling and control of hybrid UAVs," in *Proc. Int. Conf. Unmanned Aircr. Syst. (ICUAS)*, Jun. 2015, pp. 806–815.
- [35] T. Sankey, J. Donager, J. McVay, and J. B. Sankey, "UAV lidar and hyperspectral fusion for forest monitoring in the southwestern USA," *Remote Sens. Environ.*, vol. 195, pp. 30–43, Jun. 2017.
- [36] E. J. J. Smeur, M. Bronz, and G. C. H. E. de Croon, "Incremental control and guidance of hybrid aircraft applied to a tail-sitter unmanned air vehicle," *J. Guid., Control, Dyn.*, vol. 43, no. 2, pp. 274–287, Feb. 2020.
- [37] F.-P. Thamm, N. Brieger, K.-P. Neitzke, M. Meyer, R. Jansen, and M. Monninghof, "SONGBIRD—An innovative UAS combining the advantages of fixed wing and multi rotor UAS," *ISPRS-Int. Arch. Photogramm., Remote Sens. Spatial Inf. Sci.*, vol. 40, pp. 345–349, Aug. 2015.
- [38] O. Tziavou, S. Pytharouli, and J. Souter, "Unmanned aerial vehicle (UAV) based mapping in engineering geological surveys: Considerations for optimum results," *Eng. Geol.*, vol. 232, pp. 12–21, Jan. 2018.
- [39] S. Verling, B. Weibel, M. Boosfeld, K. Alexis, M. Burri, and R. Siegwart, "Full attitude control of a VTOL tail-sitter UAV," in *Proc. IEEE Int. Conf. Robot. Automat. (ICRA)*, May 2016, pp. 3006–3012.
- [40] A. Vuruskan, B. Yuksek, U. Ozdemir, A. Yukselen, and G. Inalhan, "Dynamic modeling of a fixed-wing VTOL UAV," in *Proc. Int. Conf. Unmanned Aircr. Syst. (ICUAS)*, May 2014, pp. 483–491.
- [41] W. Wang, J. Zhu, and M. Kuang, "Design, modelling and hovering control of a tail-sitter with single thrust-vectoring propeller," in *Proc. IEEE/RSJ Int. Conf. Intell. Robots Syst. (IROS)*, Sep. 2017, pp. 5971–5976.
- [42] W. Wang, J. Zhu, M. Kuang, X. Yuan, Y. Tang, Y. Lai, L. Chen, and Y. Yang, "Design and hovering control of a twin rotor tail-sitter UAV," *Sci. China Inf. Sci.*, vol. 62, no. 9, pp. 1–3, Sep. 2019.
- [43] W. Wang, J. Zhu, M. Kuang, and X. Zhu, "Adaptive attitude control for a tail-sitter UAV with single thrust-vectoring propeller," in *Proc. IEEE Int. Conf. Robot. Automat. (ICRA)*, May 2018, pp. 6581–6586.
- [44] Y. Wu, X. Du, R. Duivenvoorden, and J. Kelly, "The Phoenix drone: An open-source dual-rotor tail-sitter platform for research and education," in *Proc. Int. Conf. Robot. Automat. (ICRA)*, May 2019, pp. 5330–5336.
- [45] XMobots. *Arator 5B—The Sky Tractor, xMobots Aeroespacial—Drones for Defense and Agriculture, Web Page*. Accessed: Mar. 1, 2021. [Online]. Available: <https://xmobots.com.br/arator-5b/>
- [46] Y. Yang, J. Zhu, X. Zhang, and X. Wang, "Active disturbance rejection control of a flying-wing tail-sitter in hover flight," in *Proc. IEEE/RSJ Int. Conf. Intell. Robots Syst. (IROS)*, Oct. 2018, pp. 6390–6396.
- [47] S. Yanguo and W. Huanjin, "Design of flight control system for a small unmanned tilt rotor aircraft," *Chin. J. Aeronaut.*, vol. 22, no. 3, pp. 250–256, Jun. 2009.
- [48] J. Zhong, B. Song, Y. Li, and J. Xuan, " L_1 adaptive control of a dual-rotor tail-sitter unmanned aerial vehicle with input constraints during hover flight," *IEEE Access*, vol. 7, pp. 51312–51328, 2019.



ALYSSON NASCIMENTO DE LUCENA received two bachelor's degrees in science and technology and in mechanical engineering and the master's degree in mechanical engineering from the Federal University of Rio Grande do Norte, in 2014, 2016, and 2018, respectively. He is currently pursuing the Ph.D. degree in electrical and computer engineering with the Natalnet Associate Laboratories, Federal University of Rio Grande do Norte, where he develops aerodesign methodologies for construction of prototypes and payload techniques for unmanned Aerial vehicles. He has experience in the construction and piloting of small and medium-sized radio-controlled aircraft and micro-UAVs at the Federal University of Rio Grande do Norte.



BRUNO MARQUES FERREIRA DA SILVA (Member, IEEE) received the bachelor's degree in computer engineering and the master's and Ph.D. degrees in electrical and computer engineering from the Federal University of Rio Grande do Norte. He is currently an Associate Professor with the School of Science and Technology, Federal University of Rio Grande do Norte. He is the Co-Head of the Natalnet Associate Laboratories, where he leads research in broad computer vision research topics, particularly working with SLAM and visual odometry for mobile robot navigation and image-based 3D reconstruction.



LUIZ MARCOS GARCIA GONÇALVES (Senior Member, IEEE) received the B.Sc. degree in computer science from the State University of Rio de Janeiro, in 1993, and the Ph.D. degree in systems and computer engineering from the Computer Graphics Laboratory (LCG), COPPE-UFRJ, in 1999, including a two years stage at the Laboratory for Perceptual Robotics of UMASS at Amherst, MA, USA. He is currently a Full Professor with the Computer Engineering and Automation Department, Universidade Federal do Rio Grande do Norte, Brazil. His research interests include graphics processing, including topics as robotics vision (main interest), computer graphics, GIS, geometric modeling, animation, image processing, computer vision, and robotics in education.

...